Electron Transport in Graphene From a Diffusion-Drift Perspective

Mario G. Ancona, *Member, IEEE*

***Abstract*—A diffusion–drift treatment of electron and hole transport in macroscopic graphene is presented. The various material response functions that enter the theory are outlined and, to the extent possible, specified and calibrated. For purposes of illustration, the theory is applied to a variety of situations involving field-effect devices that are of potential technological interest. Both single and multilayer graphene are discussed, as is the effect of the small bandgaps that have been reported for graphene on SiC.**

***Index Terms*—Diffusion drift (DD), field-effect transistors, graphene, multilayer.**

I. Introduction

THE DISCOVERY that single-layer graphene is a robust material that can be isolated, contacted, and tested electrically has generated much excitement [1], [2]. Among the results obtained to date, researchers have measured mobilities as high as 250 000 $\mathrm{cm}^2/\mathrm{V}\cdot\mathrm{s}$ [3], demonstrated field-effect transistor action [1], [4]–[6], and even done an initial characterization of transport in graphene nanoribbons [7]. Most recently, intriguing evidence has been obtained for the existence of a bandgap of roughly 0.26 eV for single-layer graphene when it is formed epitaxially on SiC by sublimation of silicon at high temperature [8]–[10]. All of this activity is clearly promising, but of course, whether it will eventually lead to a practical graphene electronics technology remains to be seen. For this paper, we take the rapid progress that has been made as sufficient motivation for framing a device-oriented transport theory for graphene that may one day serve as the foundation for electronic device design and optimization tools.

Theoretical work on electron transport in graphene has generally centered on understanding ballistic or near-ballistic behaviors and on the exotic electronic properties that graphene can exhibit under ideal conditions, including when restricted in dimension as in the nanoribbons [7]. In this paper, we focus instead on the opposite limit, i.e., on developing a device modeling approach that is apropos when the transport is dominated by scattering. This interest is justified in part by the fact that except for the technologically uninteresting case of suspended exfoliated graphene [3], the mobilities measured in graphene have so far generally been far from ideal [5], [6]. It seems that, at least at present, the all-surface nature of graphene makes it particularly susceptible to nearby charges and/or localized "midgap" states [11]. While this issue is clearly in need of attention, it does imply that a graphene transport description that assumes strong scattering will be relevant at least for most research devices of today.

The conventional transport modeling approach with strong scattering is, of course, the diffusion–drift (DD) description [12]. This theory, which was developed over 50 years ago and is still the workhorse for practical semiconductor device simulation, is a macroscopic (or continuum) description in which the electron and hole populations are represented by continuous fluids or gases. The goal of this paper is to develop a similar DD description for the carrier transport in graphene.[1] Although ideal graphene is a semimetal with a markedly different band structure than an ordinary semiconductor, the basics of its DD description are not much different from the conventional theory. For one thing, we shall regard electrons in extended states above the Dirac point as forming an electron continuum, and electrons absent from extended states below the Dirac point as forming a hole continuum. Moreover, as in the conventional description, carrier motion in the graphene will be assumed to be determined by the net effect of the following three macroscopic forces: 1) the force exerted by the electrostatic field (drift); 2) the statistical pressure force arising from the random motions of the carriers (diffusion); and 3) the drag force generated by scattering that retards carrier flow through the lattice. Within this framework, the main qualitative difference between transport in graphene and in conventional semiconductors is the 2-D nature of single-layer grapheme, which precludes transport normal to the layer. (For multilayer graphene, we provide here only the lowest order treatment in which the possibility of transfer of carriers between layers is ignored, and the model therefore consists merely of an electrostatically coupled stack of single layers). As a result, the DD transport equations will be partial differential equations in 2-D. In all other respects, however, the DD equations for graphene are familiar with the remaining differences arising simply from graphene being a

Manuscript received March 17, 2009; revised November 2, 2009. Current version published February 24, 2010. This work was supported by the Office of Naval Research. The review of this paper was arranged by Editor H. S. Momose.

The author is with the Electronics Science and Engineering Division, Naval Research Laboratory, Washington, DC 20375 USA (e-mail: ancona@estd.nrl.navy.mil).

Color versions of one or more of the figures in this paper are available online at http://ieeexplore.ieee.org.

Digital Object Identifier 10.1109/TED.2009.2038644

[1]Versions of this work were presented at the International Workshop on Computational Electronics (2007) in Vienna, Austria, and at the International Conference on Simulation of Semiconductor Processes and Devices (2008) in Hakone, Japan [published in "Simulation of single and multi-layer graphene field effect devices," *Proc. SISPAD* 169 (2008)]. Work with a similar motivation has also been presented by G.I. Zebrev at the 26th International Conference on Microelectronics (2008) in Serbia [published in "Electrostatics and drift–diffusion transport in graphene field effect transistors," *Proc. Microelect.* 159 (2008)].

different "semiconductor" with a different band structure and transport properties.

Judging from its conventional counterpart, the DD theory of graphene will be rigorously justifiable when the electron/hole mean free path is small compared to the device size. The theory can therefore be expected to apply to most of the graphene test devices of current interest, which have relatively "large" geometries and are composed of low-mobility graphene [5], [6]. Beyond this, there is the well-known simplicity and robustness of the DD approach that has led to its continued utility in electronics, even when its foundational assumptions no longer seem valid. For graphene, it seems reasonable to suppose that the DD description will remain a reliable guide even for higher mobility (or even ballistic) situations since it will still incorporate the correct and often-dominant geometry, band structure effects, and electrostatics. If a graphene device technology is ever realized, the DD theory of graphene may well prove to be a useful theory and/or phenomenology for practical device design, characterization, and optimization.

II. Equations of the DD Theory of Graphene

A. Balance Laws

Assuming the electrons and holes in graphene can be regarded as continuous gases with well-defined charge and momentum densities, the partial differential equations imposed on these densities by charge conservation will take the following form:

$$\nabla \cdot \mathbf{J}_n = -R, \quad \text{where } \mathbf{J}_n = -qn\mathbf{v}_n$$
$$\nabla \cdot \mathbf{J}_p = -R, \quad \text{where } \mathbf{J}_p = qp\mathbf{v}_p. \tag{1}$$

While looking like the ordinary 3-D equations, because the carriers are restricted to be within the graphene layer (whether it is planar or not), these are 2-D equations where n and p are the areal densities (in units per square centimeter), $\mathbf{v}_n$ and $\mathbf{v}_p$ are the gas velocity vectors (in centimeters per second) lying in the 2-D surface, $\mathbf{J}_n$ and $\mathbf{J}_p$ are the current density vectors (in amperes per centimeter), R is the recombination/generation rate (in coulombs per square centimeter second), and the differential operators are surface divergences.

Scattering-dominated flow means that electron and hole inertia can be neglected and the momentum balance equations for the electron and hole gases then reduce to force balances among the three basic forces mentioned in Section I. Formulating the pressure force within each carrier gas in terms of the chemical potentials φ_n and φ_p, and assuming the drag forces per charge are proportional to the gas velocities (with the usual mobilities μ_n and μ_p as proportionality constants), we can then recast the force balances as the following DD equations:

$$\mathbf{J}_n = qn\mu_n\nabla(\varphi_n - \psi) \quad \mathbf{J}_p = -qn\mu_p\nabla(\varphi_p + \psi) \tag{2}$$

where ψ is the electrostatic potential. As with (1), the equations in (2) are familiar in form but are, again, 2-D equations with the derivatives being surface gradients within the graphene layer. When more than a single layer of graphene is present, each extra layer would be described by additional equations analogous to those in (1) and (2), and with the rate R in (1) possibly also incorporating interlayer transfer/recombination processes.

Finally, because the graphene layers are generally embedded within a 3-D device structure that includes insulators and metal contacts, the 2-D equations describing transport in the graphene must be coupled to a 3-D electrostatic equation, i.e.,

$$\nabla \cdot (\varepsilon_d \nabla\psi) = -qN_{\text{fixed}} \tag{3}$$

where N_{fixed} and ε_d are the position-dependent fixed volumetric charge density and permittivity, respectively, in the surrounding materials.

In addition to the differential equations, the basic theory must also include a consistent set of boundary conditions. In general, these are expressions of the fundamental balance laws already discussed and are derived by taking appropriate limits of integral versions of them. However, because the derivations and resulting conditions are mostly familiar [12], we omit further discussion, except to note that the crucial electrostatic condition derived from Gauss' law that relates the electric displacements across the (or each) graphene layer is

$$\mathbf{n} \cdot (\varepsilon_{d2}\mathbf{E}_2 - \varepsilon_{d1}\mathbf{E}_1) = q(p - n + N) \tag{4}$$

where the subscripts indicate values on either side of the graphene layer, $\mathbf{n}$ is the normal vector pointing from the "1" to the "2" side of the layer, and N is the effective surface charge due to any dopants, whether substitutional or adsorbed [13], or fixed charges at the layer/interface.

B. Material Response Functions

The equations in Section II-A are expressions of the general conservation laws of classical physics as applied to the electron and hole continua in graphene, assuming strong scattering (i.e., scattering forces dominating over inertial forces). In large part, they represent the physical content of the DD theory. However, as is usual in classical field theory, these equations are not complete in both physical and mathematical senses. To complete the DD theory of graphene, one must particularize various material response functions that introduce into the general equations the specific properties of graphene. It is important to note that because the growth techniques and properties of "device-grade" graphene are yet to be defined (and, indeed, may never be), optimal expressions and coefficient values for these material response functions cannot be established yet. Therefore, the functions presented herein, and their consequences discussed in subsequent sections, should be regarded merely as illustrative. As knowledge of graphene transport advances, effort should focus on better defining these response functions and on measuring their coefficient values. Of course, in the process, the range and limitations of the DD framework itself for real graphene will likely also be revealed.

The functional dependences of the material response functions that appear in the DD equations are largely set by thermodynamic considerations. This connection will not be discussed

here [14]; instead, we note only the following primary functional dependences:

$$\mathbf{D} = \mathbf{D}(\mathbf{E}, T) \tag{5a}$$

$$\varphi_n = \varphi_n(n, T) \quad \varphi_p = \varphi_p(p, T) \tag{5b}$$

$$\mu_n = \mu_n(\mathbf{v}_n, T) \quad \mu_p = \mu_p(\mathbf{v}_p, T) \tag{5c}$$

$$R = R(n, p, T). \tag{5d}$$

Of these material response functions (also known as constitutive equations), the ones for which specific expressions are most easily developed are those in (5a) and (5b) since they are nontrivial under equilibrium conditions and do not involve the nonequilibrium quantities $\mathbf{v}_n$ and $\mathbf{v}_p$.

Equation (5a) is, of course, already familiar from classical electrostatics, and its usual linear form $\mathbf{D} = \varepsilon_d \mathbf{E}$ has already been incorporated in (3) and (4). With respect to the "equations of state" in (5b), as in ordinary DD theory, their equilibrium nature allows us to utilize the powerful tools of statistical mechanics. In particular, we start with the general formula for the density of conduction electrons (with the analysis for holes being completely analogous) in uniform equilibria, i.e.,

$$n(T) = \int_0^\infty \frac{g_c(E)dE}{1 + \exp\left[(E - E_F)k_B T\right]} \tag{6}$$

where $g_c(E)$ is the 2-D density of states in the conduction band. In ideal single-layer graphene, the expression for $g_c(E)$ is [1], [15]

$$g_c(E) = \frac{2E}{\pi \hbar^2 c^2} \tag{7a}$$

where the energy is measured from the Dirac point and the Dirac electron velocity c in graphene is approximately 10^8 cm/s [1].[2] When graphene has a bandgap E_G (again, as a result of its association with SiC [8]–[10]), we employ the following approximation to the conduction band structure:

$$E(k) = \sqrt{\left(\frac{E_G}{2}\right)^2 + \hbar^2 k^2 c^2}$$

where the energy is now measured from midgap and it is assumed that both valleys remain degenerate as suggested by [9]. It is then readily shown that the conduction band density of states is given by

$$g_c(E) = \frac{2}{\pi \hbar^2 c^2} \begin{cases} 0, & E < E_G/2 \\ E, & \text{otherwise} \end{cases} \tag{7b}$$

which reduces to (7a) when E_G vanishes.

[2]In multilayer graphene, interlayer coupling can modify the band structure, as has been observed in both photoemission [T. Ohta, A. Bostwick, J.L. McChesney, T. Seyller, K. Horn, and E. Rotenberg, "Interlayer interaction and electronic screening in multilayer graphene investigated with angle-resolved photoemission spectroscopy," *Phys. Rev. Lett.* 98, 206802 (2007)] and cyclotron resonance [E.A. Henrikson, Z. Jiang, L.-C. Tung, M.E. Schwartz, M. Takita, Y.-J. Wang, P. Kim, and H.L. Stormer, "Cyclotron resonance in bilayer graphene," *Phys. Rev. Lett.* 100, 087403 (2008)]. This effect is ignored in this paper both for simplicity and because its impact is primarily at energies greater than the coupling energy estimated to be 0.39 eV.

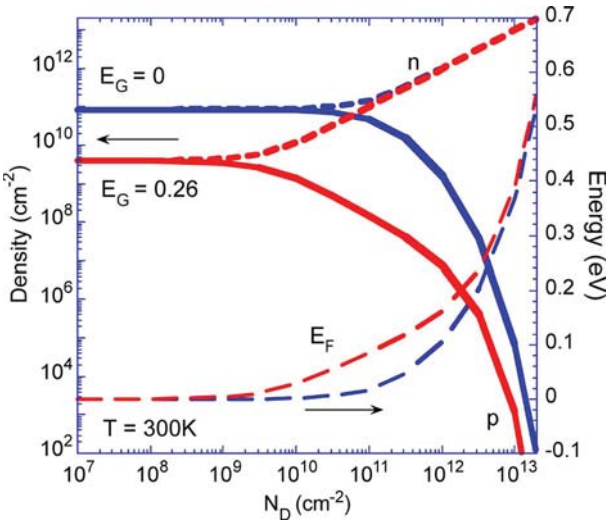

Fig. 1. Electron and hole densities and the Fermi energy versus the doping density in single-layer graphene both with the ideal zero-gap band structure and with a bandgap of 0.26 eV.

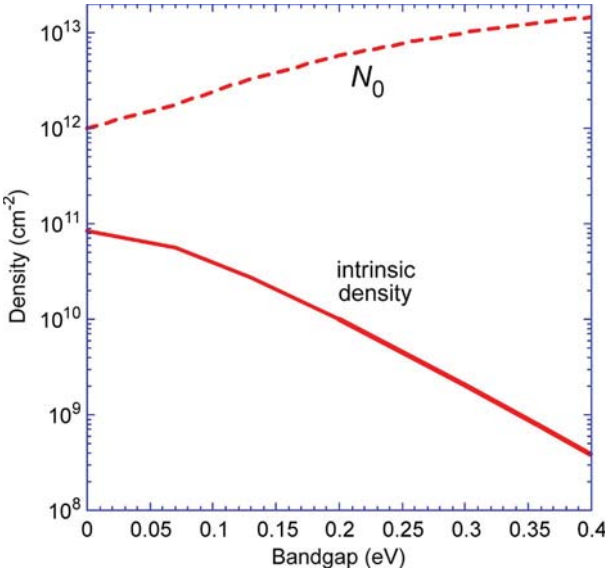

Fig. 2. Intrinsic density and the coeffcient N_0 in (8) versus bandgap in single-layer graphene.

By varying the carrier density in the graphene via doping $(N = N_D)$, we can study the relationship between density and Fermi level implied by the foregoing equations. Inserting (7b) into (6), with $E_G = 0$ eV or 0.26 eV, we obtain numerically the results shown in Fig. 1. Of course, having a bandgap is desirable from a device perspective, and this may be seen in the reduction in the intrinsic (neutral) density, as plotted in Fig. 1. More explicitly, in Fig. 2, we show the direct dependence of the intrinsic density on bandgap.

For use in the DD equations, we need an expression for $(5b)_1$ (and analogously for $(5b)_2$), and the following approximate form is easily reached by numerical inversion:

$$\varphi_n(n, T) \cong k_B T \left\{ \ln\left(\frac{n/N_{gr}}{1 + E_G/2k_B T}\right) + R\left(\frac{n/N_{gr}}{1 + N_0/n}\right)^r \right\} \tag{8}$$

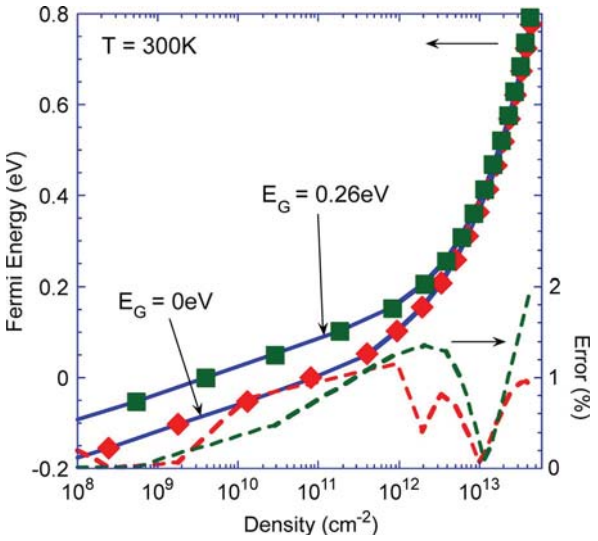

Fig. 3. Variation of the electron density as a function of either the exact chemical potential (lines) or the approximation of (8) for ideal graphene (diamonds) and graphene with a bandgap of 0.26 eV (squares). The relative errors in each case are also shown.

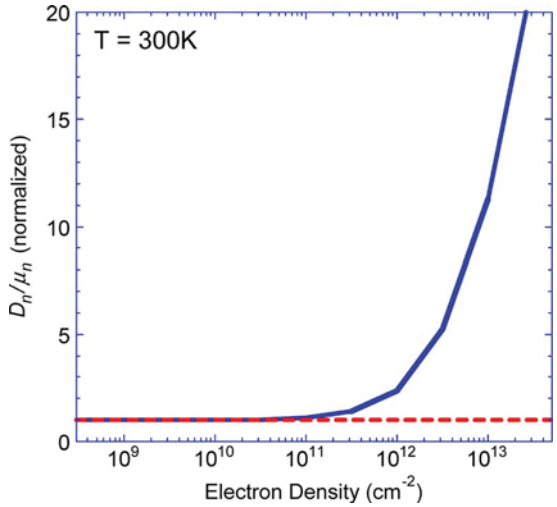

Fig. 4. Enhancement factor for diffusion in graphene due to its bandstructure.

where $r = 0.58$, $R \cong 0.69$, N_0 varies with E_G as shown in Fig. 2, and the effective density of states is $N_{gr} \equiv 2(k_B T/\hbar c)^2/\pi$ which at room temperature is approximately equal to 10^{11} cm^{-2}. As seen in Fig. 3, (8) accurately describes the electron gas for $E_G = 0$ and 0.26 eV for $n < 5 \times 10^{13}$ cm^{-2}. Due to the symmetry of the graphene band structure, one can immediately write an equation of state for holes that is directly analogous to (8). Finally, from (8), we can derive an expression for the diffusion "constant" using the formula $D_n \equiv \mu_n \partial \varphi_n / \partial n$. A plot of the diffusion "enhancement" factor D_n/μ_n is shown in Fig. 4, and as one can see, the band structure of graphene greatly amplifies the diffusivity of electrons as the density increases. We note that the widening of screening layers that would be associated with this enhanced diffusion may well have consequences for the ultimate scalability of graphene devices.

As in conventional DD theory, it is not possible to be nearly as definitive when it comes to developing expressions for the material response functions in (5c) and (5d) because of their nonequilibrium nature, and one must instead rely on complicated experimental measurements and/or theoretical calculations. Unfortunately, neither experiments (not being sufficiently comprehensive or repeatable) nor theory (not being sufficiently realistic) are presently adequate for this purpose. Therefore, in this paper, we consider only simple choices for (5c) and (5d), with the goal of illustrating the theory and with no claim that these choices are actually representative of real graphene. Presumably, as research on graphene progresses, either these forms will be confirmed or better choices can be developed.

With respect to the mobilities, two specific choices are considered. In one, we simply assume constant mobilities, for definiteness taking them to be $\mu_{n0} = \mu_{p0} = 500$ cm^2/V $\cdot$ s. This selection is particularly useful when the impact of other constitutive choices is being investigated. The other mobility model follows the conventional approach of substituting electric field for velocity and incorporates by an inverse sum a dependence on the component of the electric field normal to the graphene layer $(E_\perp)$, i.e.,

$$\frac{1}{\mu_n} = \frac{1}{\mu_{n0}}\left[1 + \left|\frac{E_\perp}{E_n}\right|^{\gamma_n}\right] \quad \frac{1}{\mu_p} = \frac{1}{\mu_{p0}}\left[1 + \left|\frac{E_\perp}{E_p}\right|^{\gamma_p}\right] \tag{9}$$

where E_n, E_p, γ_n, and γ_p are constants. In Si MOSFETs, such electric field dependences are commonly included to account for interface roughness scattering. For graphene, however, should such dependences actually prove important for describing the transport, they seem more likely to arise from scattering by fixed charges. This view is supported by the simulations of [16], [17], which suggest that small changes in the distance between the channel charge and the fixed charge (on the order of 1–2 Å) could significantly impact the scattering.

Because of graphene's zero/small bandgap, the generation–recombination term R is undoubtedly almost always important in graphene devices when they are driven out of equilibrium. Many mechanisms may be involved, but favoring simplicity, we consider just two—one associated with thermal generation and the other with band-to-band tunneling. The specific expressions we assume are

$$R_{\rm th} = \frac{np - n_{\rm eq}p_{\rm eq}}{\tau(n + p + 2\sqrt{n_{\rm eq}p_{\rm eq}})} \tag{10a}$$

$$R_{\rm tun} = \alpha\,(E_F^n - E_F^p)\,|\mathbf{E}|^\gamma \exp\left(-\frac{\beta}{|\mathbf{E}|}\right) \tag{10b}$$

where τ, α, β, and γ are constants, and the two terms combine as $R = R_{\rm th} + R_{\rm tun}$. Equation (10a) is arbitrarily assumed to be of the Shockley–Read–Hall form [12], and the band-to-band tunneling expression in (10b) is also based on conventional expressions [18]. The latter's dependence on the difference in quasi-Fermi levels ensures that it vanishes in equilibrium and that it has the proper dependence on occupancy (e.g., net recombination when $E_F^n > E_F^p$). Based on the conventional models, we assert dependences on E_G as follows:

$$\alpha = \alpha_0\sqrt{\frac{\Delta}{E_G + \Delta}} \quad \beta = \beta_0\left(\frac{E_G}{\Delta}\right)^{3/2} \quad \gamma = 2 \tag{11}$$

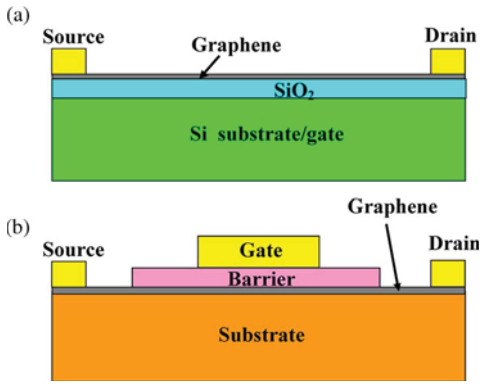

Fig. 5. Depictions of graphene field effect transistors simulated in this paper. (a) Model for the back-gated device studied in [5] and [6]. (b) Model for a front-gated device such as those formed on SiC substrates.

where α_0 and β_0 are constants, and Δ is a small constant energy ensuring that α does not become unbounded as $E_G \to 0$.

Finally, we observe that in the treatment of multilayer graphene, interlayer electron transfers would enter the theory through an additional generation–recombination term $R_{\text{interlayer}}$ (in addition to the possible band structure effects mentioned in [16]). Such transfers are ignored in this paper both for reasons of simplicity and because we believe their role to be negligible for the situations considered in this paper in which the highly conductive layers are relatively uniform and always share common contacts.

III. DD Simulations of Graphene Device Phenomena

A. Field Effect

To examine the DD treatment of the field effect in graphene, we model the particular FET studied in [5] and [6], shown schematically in Fig. 5(a). In this device, the Si substrate is doped and contacted so that it can function as a back gate. The experimentally measured drain current at low drain voltage is plotted versus the applied gate field in Fig. 6 (squares) [5], [6]. Clearly, a significant field effect is observed, but not surprisingly given the lack of a bandgap, the device displays poor turn-off characteristics. In fact, the lack of rectifying contacts results in bipolar conduction with the current merely going through a minimum as the channel switches from electron- to hole-rich, as shown in the inset in Fig. 6. Also noteworthy are the asymmetries in this characteristic both in voltage and in current.

In modeling the device in Fig. 5(a), for simplicity, we ignore possible nonuniformities in the width direction (for now) and apply the DD equations in reduced dimension, specifically solving (1) and (2) in 1-D and (3) in 2-D. These equations can be solved only numerically, and for this purpose, we transform to Slotboom variables to improve conditioning [12] and then utilize the finite-element method on a nonuniform unstructured grid. In general, the simulations always produce weak field-effect characteristics like those in Fig. 6, showing the characteristic bipolar conduction and a high OFF-state current. However, the quantitative details including the voltage/current asymmetries depend on the specific choices for the dopants,

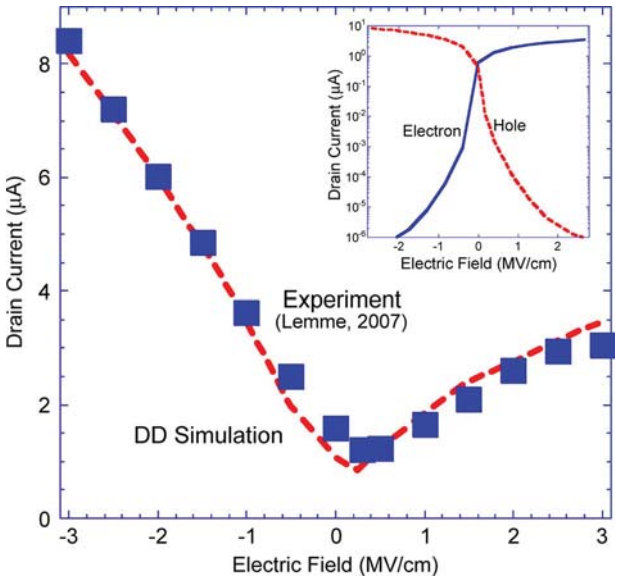

Fig. 6. Experimental data of [5], [6] and fit using a 1-D/2-D DD simulation, as discussed in the text. The inset shows the simulated electron and hole currents in the device.

the fixed charge, the contact properties, the mobility models, and the generation–recombination models. Inadequate knowledge of the device prevents us from being definitive in these choices and from identifying which of them is most important. Therefore, with illustration in mind, we simply assume that the observed threshold voltage shift is due to fixed charge at the graphene–SiO_2 interface (with $N = -10^{12}$ cm$^{-2} \to \Delta V_T = 0.4$) and, following [5] and [6], that the mobilities vary with the vertical electric field as given in (9). Furthermore, in order to provide a well-defined contact, we assume that the graphene in the vicinity of the contacts is doped n-type ($N = N_D$). That such assumptions allow DD theory to fit the data is shown in Fig. 6 (line), where we have assumed $\mu_{n0} = 1690$ cm^2/V $\cdot$ s, $\gamma_n = 0.5$, $E_n = 0.5$ MV/cm, $\mu_{p0} = 3360$ cm^2/V $\cdot$ s, $\gamma_n = 0.25$, and $E_p = 0.5$ MV/cm. Again, it is not known whether these strong electric field dependences are actually responsible for the observed behavior, but it is certainly plausible.

B. Effect of Bandgap

As noted in Section I, a bandgap is believed to be generated in graphene when it is formed epitaxially via high-temperature Si sublimation of SiC [8]–[10]. Having a bandgap is, of course, attractive because it is its lack that produces the small on/off current ratio and bipolar conduction seen in Fig. 6. That graphene on SiC is believed to have a bandgap as large as 0.26 eV [8] makes this prospect particularly intriguing, given that this is roughly the same as the bandgap of InSb, which is a material currently considered to be a legitimate candidate for future low-power digital electronics [19]. To illustrate the bandgap effect, we again study transport in an FET structure with the geometry now being that of Fig. 5(b), where the substrate is SiC and the frontside has an insulated gate situated atop the graphene. Obviously, a major effect of the bandgap is on generation–recombination, and we include this effect in the simulations using (10a) and (10b) with (11). Finally, in order

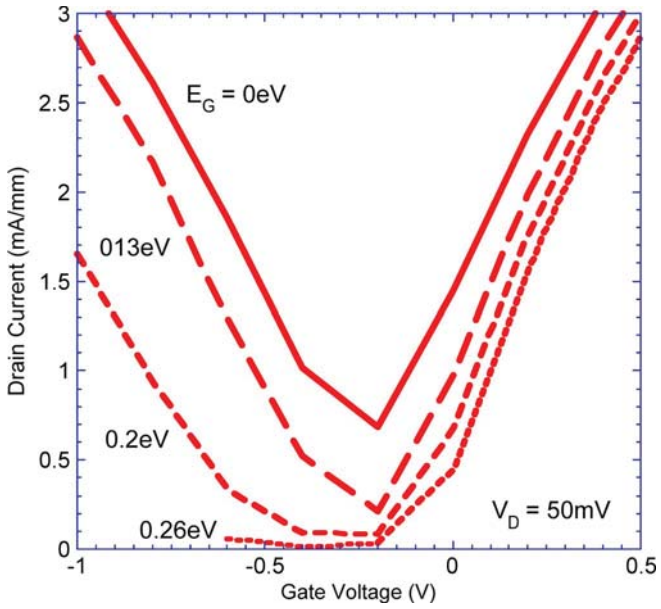

Fig. 7. DD simulation of the effect of a bandgap on the I–V characteristics of a single-layer graphene FET, with $L = 0.5$ μm and $V_D = 50$ mV.

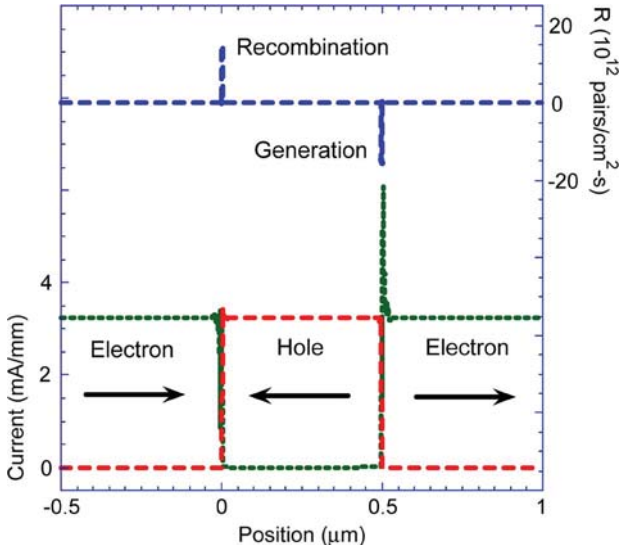

Fig. 8. Current and recombination rate as a function of source–drain bias in the FET simulated in Fig. 7 (no bandgap) and biased so that the channel is hole-rich ($V_G = -1$ V). Current flows are due to generation–recombination processes, particularly band-to-band tunneling.

not to obscure the bandgap effect with extraneous physics, we assume constant mobilities in these simulations.

The simulated transfer characteristics of the graphene FET are plotted in Fig. 7 for an applied drain voltage of 50 mV and with the bandgap treated as a parameter. Under a positive gate bias, the channel region is electron rich, current flows easily, and the bandgap has little effect. As the gate voltage is reduced, the current drops due to the field effect. However, as the bias goes negative, the effect of the bandgap becomes more pronounced. If the bandgap is nonexistent or small, then as seen earlier, strong band-to-band tunneling provides good electrical contact to the hole-rich channel and allows a bipolar current to flow. This action is depicted in profile in Fig. 8 for the case with zero bandgap. However, when the bandgap becomes larger,

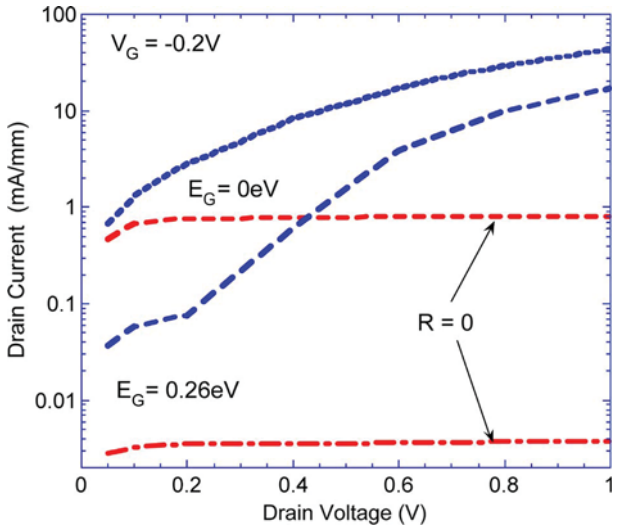

Fig. 9. Drain characteristics with and without carrier generation–recombination and showing the effect of the bandgap in reducing multiplication.

the decline in band-to-band tunneling strongly suppresses the current under negative bias, as seen in Fig. 7. Indeed, for bandgaps greater than about 0.26 eV, the FET exhibits good turn-off characteristics with increasingly large on/off current ratios. In these cases, the off-current seen in Fig. 7 is largely due to the abruptness of the source–drain contact doping profile.

One additional effect of the small bandgap is carrier multiplication under a high drain bias. For purposes of illustration, we assume that this phenomenon occurs solely via the generation processes included in (10a) and, more particularly, (10b). Simulation results comparing the currents with and without generation included and for several bandgaps are shown in Fig. 9. Not surprisingly, having a bandgap strongly suppresses the multiplication effect as well, particularly at a low drain voltage.

C. Effect of Multilayers

To illustrate the DD simulation of transport in multilayer graphene, we again assume an FET structure like that of Fig. 5(b), but now with the current flowing in a stack of four graphene layers, all identically contacted at the source and drain and all with identical constant mobilities. As noted earlier, we assume in this paper that the transfer of carriers between layers is impossible, and to model the electrostatic interactions explicitly, we assume that the layers are separated by a very small distance, with the condition in (4) applied across each individual layer.[3] The separation distance was assumed to be either 0.35 nm (the actual value) or 1.0 nm (a relaxed value that eases mesh requirements), and not surprisingly, both values give essentially the same results. Simulations are carried out just as before, and in Fig. 10, we exhibit the resulting gate characteristics, plotting the current carried in each individual layer for the case when all layers have zero bandgap. The

[3]This calculation is therefore the macroscopic analog of that of P.B. Visscher and L.M. Falicov, "Dielectric screening in a layered electron gas," *Phys. Rev. B* **3**, 2541 (1971).

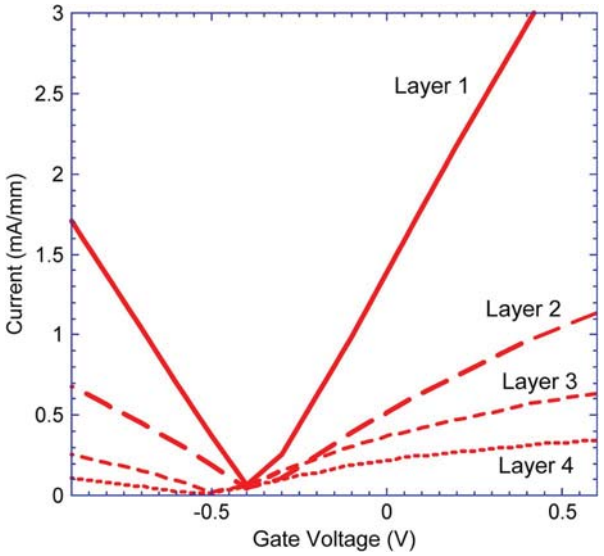

Fig. 10. DD simulation of the current contributions from the individual layers in a four-layer graphene FET as a function of gate voltage. In this simulation, all the layers are assumed to have zero bandgap.

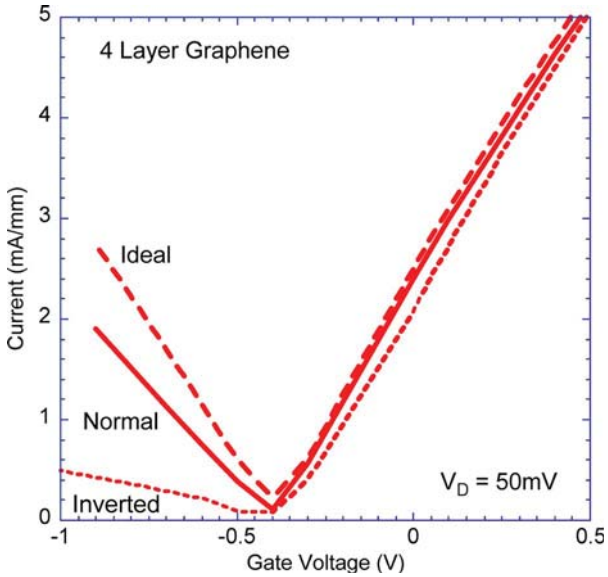

Fig. 11. DD simulation of the total current in a four-layer zero-gap graphene FET as a function of gate voltage.

behavior is readily understood. For gate voltages near threshold (in this case, $V_T \sim -0.4$ V), the intrinsic density in each layer leads each to contribute roughly equally, while at a higher bias (either positive or negative), the accumulation of electrons or holes in the layer closest to the gate causes it to screen out the other layers and to be increasingly dominant. From the perspective of materials characterization, this observation may be of value in that it means that the single (topmost) layer conduction can be monitored, even when multilayers are present and simultaneously contacted.

As noted earlier, studies of graphene formed on SiC suggest that an energy bandgap is opened up due to the presence of the SiC [8]. These studies further indicate that for multilayer graphene the induced bandgap decreases in the layers more distant from the SiC with the approximate values for the bandgaps reported in [8] as follows: first layer, 0.26 eV; second layer, 0.14 eV; third layer: 0.066 eV; and fourth layer: 0.02 eV. As a second multilayer calculation, we compare in Fig. 11 the transfer characteristics for four-layer graphene with no bandgap (labeled "ideal") with two additional simulated curves (labeled "normal" and "inverted") in which the realistic variable bandgaps on SiC have been included. The "normal" curve refers to a device like that of Fig. 5(b) in which the SiC is the device substrate and the gate barrier is a deposited material such as SiO_2, whereas the "inverted" case has the SiC on which the graphene has formed as the barrier layer and the device substrate being a deposited or wafer-bonded material. To our knowledge, the latter "inverted" structure has not yet been explored experimentally, but as Fig. 11 shows, the situation is interesting because it shows a potential for significant turn-off despite the graphene stack including zero-bandgap layers. To understand how this can be, we observe first that under a positive bias, the currents for all cases are nearly the same because, as seen earlier, the bandgap has little effect when the conduction is entirely by majority carriers (in this case, electrons). However, as we saw in Figs. 7 and 8, under a negative bias, the current flow depends on strong generation–recombination, which is suppressed when a significant bandgap is present. In the "normal" case, the layer with the biggest bandgap is *farthest* from the gate, and, therefore the current suppression is of least consequence since this carries minimal current anyway due to the screening (as shown in Fig. 10). On the other hand, in the "inverted" case, the bandgap is in the layer closest to the gate, and therefore, suppression of its current will have a big effect since this layer is the dominant carrier of current (except near threshold) because of screening.

Another way of looking at the results in Fig. 11 is to compute the ratios of the currents in the ON and OFF states. If we assume that $V_{\rm DD} = 1.5$ V and use a "2:1" rule [21] to define $V_{\rm ON} = V_T + 1$ V and $V_{\rm OFF} = V_T - 0.5$ V, then for $V_D = 50$ mV, we obtain the following $I_{\rm ON}/I_{\rm OFF}$ ratios: zero gap, 3.9; "normal," 3; and "inverted," 13. Obviously, from a device perspective, the "inverted" case is best, and while not ideal, it might provide the simplest route to "useful" graphene devices. In addition, as noted before, it could also serve as a means for better characterizing graphene-on-SiC material in nonideal multilayer samples.

D. *Effect of Lateral Nonuniformities*

In ultrasmall-geometry FETs, an important technological issue is the impact of random dopants/charges in producing significant device-to-device variations in threshold voltage. Given the all-surface nature of graphene, one might expect such an issue to be even more important in graphene devices [16], [17]. In this paper, we do not explore this issue at all; instead, we simply use it as a means of illustrating the DD theory of graphene in a 3-D situation. To this end, we insert a random distribution of fixed charges into a 3-D version of the device shown in Fig. 5(a) and then simulate it by solving the equations of our DD theory, namely, (1) and (2) solved in 2-D and (3) solved in 3-D. A result from these simulations is plotted in Fig. 12, where we show the electron density as a function of

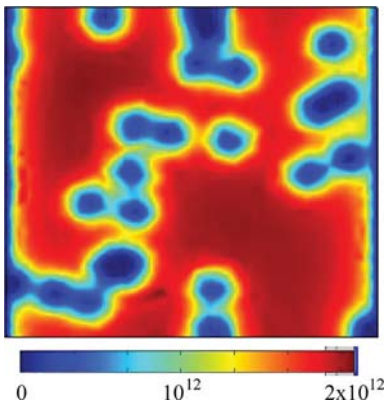

Fig. 12. Electron density in a channel with randomly positioned fixed charges in a 2-D/3-D DD graphene simulation. The region shown is 50 nm × 50 nm in size.

position in the channel of a small-geometry FET. Perhaps most noteworthy is the small size of the perturbations induced by the charges as a result of their being in very close proximity to the 2-D graphene layer. This suggests that the effect of lateral nonuniformities in graphene might actually be less than in conventional FETs. It is also reminiscent of the experimental observations of Martin [21].

IV. Final Remarks

This paper has introduced a DD theory that describes electron and hole transport in single and multilayer graphene. The main difference in formulation from ordinary DD theory stems from the 2-D nature of macroscopic grapheme, which causes the new theory to be a hybrid of 2-D transport equations and 3-D electrostatics. The other differences from conventional theory are more quantitative in nature and largely result from the different band structure of graphene. In other words, in this respect, graphene is merely a different "semiconductor." The graphene properties enter the theory through material response functions that we described first in a general fashion and then by proposing some specific forms. Given the presently incomplete state of knowledge about graphene, the best understood of these functions are the equations of state for electrons and holes, and we provide expressions both for the case of ideal graphene with zero bandgap and for graphene that has a bandgap as is believed to occur when it is formed on SiC. New and more tentative constitutive models for the mobilities and for generation/recombination by thermal means and by band-to-band tunneling were also proposed. The DD theory of graphene was then illustrated using numerical simulations that exhibited its treatments of field-effect situations, the effect of bandgap, the effect of multilayers, and the effect of lateral nonuniformities.

Altogether, the DD theory of graphene is quite familiar, and given the close analogy to ordinary DD theory, it is obviously well suited to device modeling, particularly for fast-turnaround engineering applications. In this use, it is important that one be aware of the chief foundational assumption of the theory, which is that the carrier mean free path is presumed to be "short" compared to the device size. This means that it is best applied to larger device geometries and to relatively low mobility graphene like most present-day material. Beyond this, however, experience with conventional DD theory suggests that the graphene theory will be robust and likely useful well beyond its supposed range of applicability, particularly when used as an engineering phenomenology. Additionally, just as conventional DD theory is often extended to apply to transport in confined geometries (e.g., quantum wells), so might our graphene transport theory be generalized to treat transport in the quantum-confined regime, e.g., to graphene nanoribbons. Of course, whether any of this is ever important depends on the extent to which graphene matures as an electronic material in the coming years.

Acknowledgment

The author would like to thank Dr. C. Baatar and Dr. B. V. Shanabrook for helpful comments.

References

[1] K. C. Novoselov, A. K. Geim, S. V. Morozov, D. Jiang, Y. Zhang, S. V. Dubonos, I. V. Grigorieva, and A. A. Firsov, "Electric field effect in atomically thin carbon films," *Science*, vol. 306, no. 5696, pp. 666–669, Oct. 2004.

[2] C. Berger, Z. M. Song, T. B. Li, X. B. Li, A. Y. Ogbazghi, R. Feng, Z. T. Dai, A. N. Marchenkov, E. H. Conrad, P. N. First, and W. A. de Heer, "Ultrathin epitaxial graphite: 2D electron gas properties and a route toward graphene-based nanoelectronics," *J. Phys. Chem. B*, vol. 108, no. 52, pp. 19 912–19 916, Dec. 2004.

[3] K. I. Bolotin, K. J. Sikes, Z. Jiang, M. Klima, G. Fudenberg, J. Hone, P. Kim, and H. L. Stormer, "Ultrahigh electron mobility in suspended graphene," *Solid State Commun.*, vol. 146, no. 9/10, pp. 351–355, Jun. 2008.

[4] B. Huard, J. Sulpizio, N. Stander, K. Todd, B. Yang, and D. Goldhaber-Gordon, "Transport measurements across a tunable potential barrier in graphene," *Phys. Rev. Lett.*, vol. 98, no. 23, p. 236 803, Jun. 2007.

[5] M. C. Lemme, T. Echtermeyer, M. Baus, and H. Kurz, "A graphene field-effect device," *IEEE Electron Device Lett.*, vol. 28, no. 4, pp. 282–284, Apr. 2007.

[6] M. C. Lemme, T. Echtermeyer, M. Baus, B. Szafranek, J. Bolten, M. Schmidt, T. Wahlbrink, and H. Kurz, "Mobility in graphene double-gate field-effect transistors," *Solid-State Electron.*, vol. 52, no. 4, pp. 514–518, Apr. 2008.

[7] M. Y. Han, B. Ozyilmaz, Y. Zhang, and P. Kim, "Energy band-gap engineering of graphene nanoribbons," *Phys. Rev. Lett.*, vol. 98, no. 20, p. 206 805, May 2007.

[8] S. Y. Zhou, G. H. Gweon, A. V. Federov, P. N. First, W. A. de Heer, D. H. Lee, F. Guinea, A. Neto, and A. Lanzara, "Substrate-induced bandgap opening in epitaxial graphene," *Nat. Mater.*, vol. 6, no. 10, pp. 770–775, Oct. 2007.

[9] S. Kim, J. Ihm, H. J. Choi, and Y.-W. Son, "Origin of anomalous electronic structures of epitaxial graphene on silicon carbide," *Phys. Rev. Lett.*, vol. 100, no. 17, p. 176 802, May 2008.

[10] E. Rotenberg, A. Bostwick, T. Ohta, J. L. McChesney, T. Seyller, and K. Horn, "Origin of the energy bandgap in epitaxial graphene," *Nat. Mater.*, vol. 7, no. 4, pp. 258–259, Apr. 2008.

[11] T. Stauber, N. Peres, and F. Guinea, "Electronic transport in graphene: A semi-classical approach including midgap states," *Phys. Rev. B, Condens. Matter*, vol. 76, no. 20, p. 205 423, Nov. 2007.

[12] S. Selberherr, *Analysis and Simulation of Semiconductor Devices*. Vienna, Austria: Springer-Verlag, 1984.

[13] T. O. Wehling, K. S. Novoselov, S. V. Morozov, E. E. Vdovin, M. I. Katsnelson, A. K. Geim, and A. I. Lichtenstein, "Molecular doping of graphene," *Nano Lett.*, vol. 8, no. 1, pp. 173–177, Jan. 2008.

[14] M. G. Ancona and H. F. Tiersten, "Fully macroscopic description of bounded semiconductors with an application to the Si-SiO_2 interface," *Phys. Rev. B, Condens. Matter*, vol. 22, no. 12, pp. 6104–6119, Dec. 1980.

[15] P. R. Wallace, "The band theory of graphite," *Phys. Rev.*, vol. 71, no. 9, pp. 622–634, May 1947.

[16] E. H. Hwang, S. Adam, and S. Das Sarma, "Carrier transport in two-dimensional graphene layers," *Phys. Rev. Lett.*, vol. 98, no. 18, p. 186 806, May 2007.

[17] S. Adam, E. H. Hwang, V. M. Galitski, and S. Das Sarma, "A self-consistent theory for graphene transport," *Proc. Nat. Acad. Sci.*, vol. 104, no. 47, pp. 18 392–18 397, Nov. 2007.

[18] G. Hurkx, H. de Graaff, W. Kloosterman, and M. Knuvers, "A new analytical diode model including tunneling and avalanche breakdown," *IEEE Trans. Electron Devices*, vol. 39, no. 9, pp. 2090–2098, Sep. 1992.

[19] M. Radosavljevic, T. Ashley, A. Andreev, S. D. Coomber, G. Dewey, M. T. Emeny, M. Fearn, D. G. Hayes, K. P. Hilton, M. K. Hudait, R. Jefferies, T. Martin, R. Pillarisetty, W. Rachmady, T. Rakshit, S. J. Smith, M. J. Uren, D. J. Wallis, P. J. Wilding, and R. Chau, "High-performance 40 nm gate length InSb p-channel compressively-strained quantum well field-effect transistors for low-power logic applications," in *IEDM Tech. Dig.*, 2008, p. 727.

[20] R. Chau, J. Brask, S. Datta, G. Dewey, M. Doczy, B. Doyle, J. Kavalieros, B. Jin, M. Metz, A. Majumdar, and M. Radosavljevic, "Application of high-kappa gate dielectrics and metal gate electrodes to enable silicon and non-silicon logic nanotechnology," *Microelectron. Eng.*, vol. 80, pp. 1–6, Jun. 2005.

[21] J. Martin, N. Akerman, G. Ulbricht, T. Lohmann, J. H. Smet, K. von Klitzing, and A. Yacoby, "Observation of electron-hole puddles in graphene using a scanning single-electron transistor," *Nat. Phys.*, vol. 4, no. 2, pp. 144–148, Feb. 2008.

Mario G. Ancona (M'79) received the B.E.S. degree from Johns Hopkins University, Baltimore, MD, and the M.S. and Ph.D. degrees from Rensselaer Polytechnic Institute, Troy, NY.

He has been a Member of Staff of the Electronics Science and Engineering Division, Naval Research Laboratory, Washington, DC, for 25 years, where he has worked in many areas of semiconductor device physics, modeling, and engineering. He is also the author of the book *Computational Methods for Applied Science and Engineering* (Rinton Press, Princeton, NJ, 2002).